Iron self-diffusion in FeZr/^{57}FeZr multilayers measured by neutron reflectometry: Effect of applied compressive stress

Mukul Gupta,[1,2,*] Ajay Gupta,[1] Sujoy Chakravarty,[1] Rachana Gupta,[1,2] and Thomas Gutberlet[2]
[1]*UGC-DAE Consortium for Scientific Research, Khandwa Road, Indore, 452017, India*
[2]*Laboratory for Neutron Scattering, ETH Zürich and Paul Scherrer Institute, CH-5232 Villigen PSI, Switzerland*
(Received 31 January 2006; revised manuscript received 12 June 2006; published 21 September 2006)

Iron self-diffusion in nanocomposite FeZr alloy has been investigated using a neutron reflectometry technique as a function of applied compressive stress. A composite target of Fe+Zr and ^{57}Fe+Zr was alternatively sputtered to deposit chemically homogeneous multilayer (CHM) structure $[^{natural}Fe_{75}Zr_{25}/^{57}Fe_{57}Zr_{25}]_{10}$. The multilayers were deposited onto a bent Si wafer using a three-point bending device. Post-deposition, the bending of the substrate was released which results in an applied compressive stress on to the multilayer. In the as-deposited state, the alloy multilayer forms an amorphous phase, which crystallizes into a nanocomposite phase when heated at 373 K. Bragg peaks due to isotopic contrast were observed from CHM, when measured by neutron reflectivity, while x-ray reflectivity showed a pattern corresponding to a single layer. Self-diffusion of iron was measured with the decay of the intensities at the Bragg peaks in the neutron reflectivity pattern after thermal annealing at different temperatures. It was found that the self-diffusion of iron slows down with an increase in the strength of applied compressive stress.

DOI: 10.1103/PhysRevB.74.104203 PACS number(s): 66.30.Fq

I. INTRODUCTION

During recent decades amorphous and nanocrystalline metals and alloys have been investigated as an important class of materials with the possibility of tailoring their properties over a wide range by controlling particle size and morphology.[1–4] More recently nanocomposite alloys, in which nanocrystals are surrounded by an intergranular amorphous matrix, have attracted great attention due to their interesting structural[5] and magnetic properties.[6–8] One favorable way to obtain a nanocomposite alloy, is partial crystallization of the amorphous alloy.[2,9,10] The alloy structure obtained above the primary crystallization temperature of the parent amorphous phase, but below the secondary crystallization temperature, has been termed a nanocomposite phase.[11] Above the secondary crystallization temperature, the nanocomposite structure fully crystallizes to form an equilibrium state of the alloy. Structurally, the nanocrystals obtained after primary crystallization are surrounded by an amorphous intergranular phase to form a nanocomposite phase.[1,12] Nanocomposite alloys produced with an amorphous precursor are the basis of interesting soft-magnetic alloys known as FINEMET (Ref. 13), NANOPERM (Ref. 14), and HITPERM (Ref. 15). Since the nanocomposite phases produced in these alloys is inherently a metastable phase, diffusion of the constituents would play an important role in understanding and determining their properties for long-standing applications. Hence, atomic diffusion in such alloys is the key phenomenon for selecting their applications.[16]

The situation becomes more complicated when the nanocomposite alloys are produced in the form of a thin film. Deposition of thin films onto a substrate is known to produce films with a large intrinsic strain or stresses which often result from the differences in thermal expansion (thermal stress) or from the microstructure of the deposited film (intrinsic stress).[17–19] The intrinsic stresses may originate due to several factors: (i) at the strained regions within the films, e.g., grain-boundaries, dislocations, voids, impurities, etc., (ii) at the film/substrate interface due to lattice mismatch, different thermal expansion, etc., (iii) at the film/vacuum interfaces due to surface stress, adsorption, etc., or (iv) due to dynamic processes, e.g., recrystallization, interdiffusion, etc.[20] These stresses may significantly affect the physical properties of the thin films, including atomic diffusion.

It is known that when a material is deposited in the thin film state, the diffusivity can be completely different as compared to bulk state of that material, even when the material is in purely elemental form. Such a behavior has been mainly attributed to an increased defect concentration, metastability, and unrelaxed state of the material. Therefore an extrapolation of bulk diffusivity may result in erroneous values of diffusivity in the case of thin films. Since many devices which are used for application are fabricated in the form of nm range thin films, self-diffusion measurements can be extremely important for their applications.

In order to study the nature of stresses on self-diffusion we have chosen a simple binary FeZr alloy for this purpose. It was found that (as will be shown later) after annealing at 373 K, the alloy forms a nanocomposite phase which further crystallizes above 600 K. The self-diffusion of iron was measured in the nanocomposite state as a function of applied stress. The samples were deposited onto a substrate with a known bending. An external stress on to a $[^{natural}Fe_{75}Zr_{25}/^{57}Fe_{57}Zr_{25}]_{10}$ multilayer was applied by releasing the bending of the substrate which resulted in an applied compressive stress. Iron self-diffusion measurements were carried out using a neutron reflectivity technique. It may be noted that the neutron reflectivity is an excellent technique for studying self-diffusion in nm range structures. Due to the fact that neutron scattering length densities for isotopes of an element are different, neutron reflectivity with depth resolution in the sub nm range provides a unique opportunity for measuring self-diffusion. Conventional cross-sectioning and depth-profiling techniques, such as ra-

diotracer, secondary ion mass spectroscopy (SIMS) are not suitable for measuring self-diffusion in nm range structures as the depth resolution available with cross-sectioning and depth-profiling techniques is of the order of a few nm.

In an earlier work[21] we demonstrated that neutron reflectivity is a technique which could be used to probe diffusion lengths of the order of 0.1 nm, and diffusion at temperatures less than 400 K could be measured. In the present work, the effect of compressive stress on the self-diffusion of iron in nanocomposite multilayers was studied using neutron reflectivity.

II. SAMPLE PREPARATION AND CHARACTERIZATION

FeZr, CHM were deposited on Si (100) substrates using a magnetron sputtering technique. Small pieces of Zr rods were pasted on the ^{natural}Fe and ^{57}Fe targets in a symmetric way and the composite targets were sputtered alternately to prepare a chemically homogeneous structure with a nominal composition $Si/[^{natural}Fe_{75}Zr_{25}(25\ nm)/^{57}Fe_{75}Zr_{25}(10\ nm)]_{10}$. The deposition of the multilayer was carried out after obtaining a base pressure better than 1×10^{-6} mbar. During the deposition, pressure in the chamber was 5×10^{-3} mbar due to 30 cm^3/min Ar gas flow used for sputtering of the targets. All the samples were deposited at a constant sputtering power of 50 W. Before deposition the vacuum chamber was repeatedly flushed with Ar gas so as to minimize the contamination of the remaining gases present in the chamber. Both the targets were presputtered at least for 10 min. During the deposition the substrate was mounted on a specially designed three-point Si wafer bending device. The substrate was oscillated with respect to central position of the target for better uniformity of the thickness of the deposited sample.

In all the cases, thin Si wafers (300 ± 10) μm were used as a substrate in order to avoid breaking during bending. The Si wafer was fixed from both the ends, and by rotation of an asymmetric roller around the central axis, the bending height of the Si wafer can be varied between 0 to 5 mm. A pin-lock system was incorporated so that release of bending by itself could be avoided. A compressive stress (uniaxial) is applied onto the deposited film, when the bending of the Si wafer was released after deposition. The applied stress due to release of bending onto the Si wafer can be calculated using Stoney's formula[22] and following a discussion given by Chen *et al.*[23] The applied stress σ is given by:

$$\sigma = \frac{\left(\frac{E_{Si}}{1-\nu_{Si}}\right)T_{Si}^2}{6RT_f}, \tag{1}$$

where $\left(\frac{E_{Si}}{1-\nu_{Si}}\right)$ is the biaxial modulus of the silicon substrate and is equal to 180.5 GPa. E_{Si} is Young's modulus for Si and ν_{Si} is Poisson's ratio for Si. T_{Si} is the thickness of the substrate, T_f is the thickness of the film, and R is the radius of curvature. With the situation shown in Fig. 1, the radius of curvature can be written:

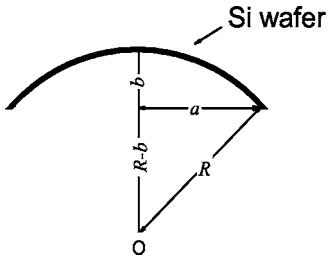

FIG. 1. Schematic diagram of the bent Si wafer, used for calculation of radius of curvature.

$$R = \frac{a^2+b^2}{2b}. \tag{2}$$

Combining Eqs. (1) and (2), the value of stress was calculated. The parameters used in the present case are $T_{Si}=(300\pm10)$ μm, $T_f=370$ nm, $a=40$ mm, and b was varied at 0, 3, and 5 mm. The obtained values of stress for the 3 cases are 0, 27, and 46 GPa. The errors in the calculation of applied stress were of the order of 15–20%, taking into account the uncertainties in the measured physical parameters. Samples with different known bending were deposited under similar deposition conditions. After deposition and release of bending, the surface profile of the samples was measured using a profilometer. It was found that the surface of the samples was flat and no changes in the surface profile were observed for a sample prepared with or without bending. This indicated that even after the bending the substrate gains its original state and the stress is applied onto the deposited multilayer.

The composition of the deposited films was determined using x-ray photoelectron spectroscopy (XPS) depth profiling. The XPS profile was measured using monochromatic Al Kα x-rays (1 mm spot size) at the surface and at three different depths, after sputtering with Ar ions of 1 mA current and 3 kV accelerating voltage. The pressure during measurements was better than 1×10^{-8} mbar. The average composition of the films was equal to $Fe_{75\pm3}Zr_{25\pm3}$, excluding the data taken at the surface. Since at the surface contributions from absorbed species like carbon and oxygen were significant, the average composition of the film was determined with the data taken at three different depths. It was found that at the surface and near surface regions have oxygen content as high as 40%; however, as the sample was sputtered the oxygen content decreased drastically and on an average remained constant at 6%.

Structural characterizations of the samples were carried out with x-ray reflectivity (XRR) and grazing incidence diffraction using a standard x-ray diffractometer (XRD) with Cu Kα x-rays. The crystallization behavior of the multilayers was examined using differential scanning calorimetry (DSC) with NETZSCH, DSC equipped with extremely high sensitivity μ sensor. The conversion electron Mössbauer spectroscopy measurements (CEMS) were performed for determining the local environment of ^{57}Fe in the samples. The measurements were carried out using a 50 mCi ^{57}Co-radiactive source in a Rh matrix and a gas flow proportional counter (He+4%CH_4) for detection of conversion

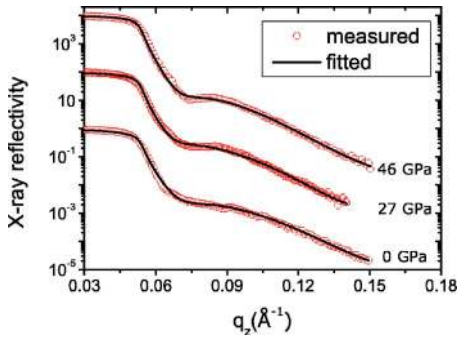

FIG. 2. (Color online) X-ray reflectivity of the as-deposited Si/[^{natural}Fe$_{75}$Zr$_{25}$(25±1 nm)/^{57}Fe$_{75}$Zr$_{25}$(12±1 nm)]$_{10}$ multilayer at different applied stresses. The intensity shown on *y* axis has been multiplied by a factor of 100, for clarity.

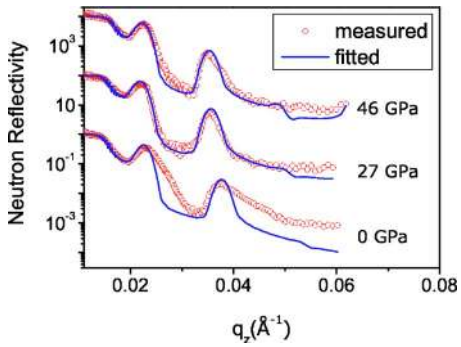

FIG. 3. (Color online) Neutron reflectivity of the as-deposited Si/[^{natural}Fe$_{75}$Zr$_{25}$(25±1 nm)/^{57}Fe$_{75}$Zr$_{25}$(12±1 nm)]$_{10}$ multilayer prepared with applied stresses of 0, 27, and 46 GPa. The intensity shown on *y* axis has been multiplied by a factor of 100, for clarity.

electrons. The isomer shifts were calibrated relative to α-Fe. Hysteresis loops as a function of azimuthal angle were measured using a magneto-optical Kerr effect (MOKE).

Self-diffusion measurements were performed using a neutron reflectometry technique at a reflectometer known as AMOR, situated at the Swiss spallation neutron source (SINQ), at Paul Scherrer Institute, Switzerland.[24] The reflectivity pattern was measured using two different angular settings (0.5° and 1.0°) in the time-of-flight mode.

III. RESULTS AND DISCUSSION

A. Structural properties

The multilayers prepared in this work have a periodicity only for iron isotopes; it is expected that x-ray reflectivity of the multilayers would show a pattern corresponding to a single layer. Figure 2 shows an x-ray reflectivity pattern of the multilayer structure prepared at 0, 27, and 46 GPa. As can be seen from the pattern, at the designed period of the multilayer there was no contrast for x-rays, which confirms the chemical homogeneity of the layers. The x-ray reflectivity pattern was fitted assuming a single layer and an "oxide" layer of about 6 nm thickness on the surface of the multilayer, using a computer program based on Parratt's formalism.[25] Such an oxide layer on the surface of the sample may stem from absorbed oxygen or other light elements, when the samples are exposed to the atmosphere after deposition. Presence of such a layer was also evident from XPS measurements.

On the other hand the neutron reflectivity pattern (Fig. 3) showed well-pronounced Bragg peaks arising due to isotopic contrast between ^{natural}Fe and ^{57}Fe. As can be seen from the figure, the sample prepared without any stress showed rather asymmetric Bragg peaks, while for the samples prepared with an applied stress, the peaks were more symmetric. Such an asymmetry of the Bragg peaks may arise due to incorporation of some free volume which may result in some internal strain or stresses during the growth of the film and might cause an asymmetry in the scattering length density. For the samples which were prepared in the bent state, the release of bending results in an applied external stress on the multilayer which eventually results in annihilation of free volume. The fitting of the data was obtained assuming symmetrical distribution of the number density across the layer which results in marked differences with the data obtained for the sample prepared without an applied stress. The neutron reflectivity pattern was fitted using a computer program based on Parratt's formalism[25] and it was found that the pattern could not be fitted assuming sharp interfaces; instead a thin interlayer of thickness (1±0.5) nm with the mean scattering length density of the two layers had to be introduced as an interdiffused layer. This means that already at room temperature there is some amount of interdiffusion in the multilayer. The fitted parameters give the structure of the multilayers: Si / [^{natural}Fe$_{75}$Zr$_{25}$(25 ± 1 nm) /^{57}Fe$_{75}$Zr$_{25}$(12 ± 1 nm)]$_{10}$, which is close to the nominal structure.

B. Crystallization behavior

Prior to diffusion measurements thermal stability of the samples was studied with grazing incidence x-ray diffraction. All the samples were annealed together in a vacuum furnace in the temperature range of 373–573 K with 100 K step for about 60 min. In the as-prepared state all the samples show a diffuse maxima centered around 2θ=44.6°, with a width of about 4–5° (see Fig. 4), which means that the samples are x-ray amorphous in the as-prepared state. The width of the diffuse maxima is comparable to the iron based amorphous alloys.[2] The average interatomic distance can be estimated using the relation[26] $a=1.23\lambda/2 \sin\theta$, where θ is taken to be the angle at the center of the diffuse maxima, and the factor 1.23 is a geometric factor which rationalizes the nearest neighbor distance with the spacing between "pseudo-close packed planes." As shown in Fig. 4, with an increase in the applied stress the position of the amorphous maxima shifts toward a higher angle side indicating a decrease in the average interatomic distance as shown in the inset of the figure. Such a decrease in the average interatomic distance may be caused due to applied compressive stress. After annealing at 373 K, the broad hump becomes narrow (width ~1°) and a nanocomposite structure is found, as shown in Fig. 5. The peak shape from the nanocomposite structure could be fitted only by deconvoluting it into two lines, one corresponding to the parent amorphous phase and the second to a nanocrystal-

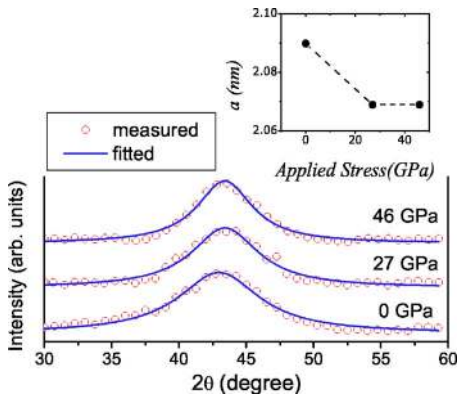

FIG. 4. (Color online) X-ray diffraction pattern of the isotopic multilayers in the as-deposited state. The measurements were carried out in the grazing incidence geometry using Cu Kα x-rays. The inset in the figure shows the change in interatomic distance (a) as a function of applied stress.

line bcc-Fe phase. The area ratio of amorphous phase as determined from the fitting of XRD data was in the range of 15–25%. A slight decrease in the area ratio of the amorphous phase was observed for the samples prepared with an applied stress. On further annealing at 473 and 573 K, no significant changes in the XRD pattern of the samples were observed as shown in Fig. 5. After annealing at different temperatures the position of the Bragg peak shifts toward a higher angle indicating a further decrease in the interatomic spacing. Such a decrease in interatomic spacing is related to structural relaxation and is a consequence of annihilation of free volume. The grain size of the nanocrystals was about 10 nm, which increases marginally with an increase in the annealing temperature as shown in Fig. 6.

Crystallization behavior of the samples was also studied using conversion electron Mössbauer spectroscopy (CEMS).

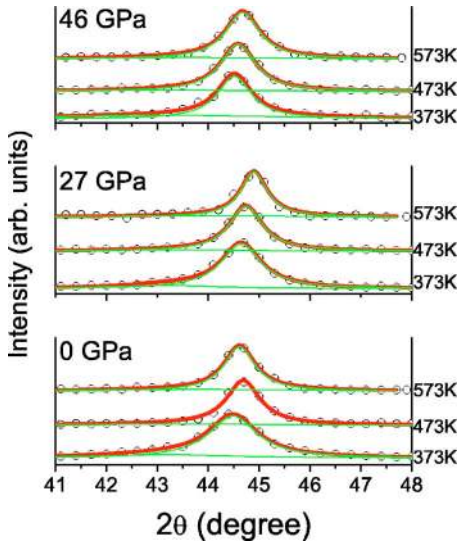

FIG. 5. (Color online) Grazing incidence x-ray diffraction pattern of Si/[$^{natural}Fe_{75}Zr_{25}$(25±1 nm)/$^{57}Fe_{75}Zr_{25}$(12±1 nm)]$_{10}$ multilayer prepared with an applied stress of 0, 27, and 46 GPa after annealing at different temperatures. Open circles represent the measured data and the solid lines are fit to them.

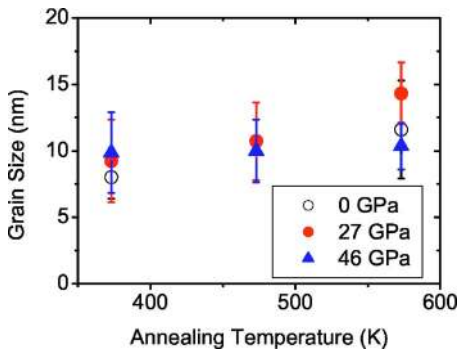

FIG. 6. (Color online) Average grain size as a function of annealing temperature shown representatively for a sample prepared with an applied stress of 0, 27, and 46 GPa.

Samples prepared with and without applied stress were annealed at high temperatures. Figure 7 compares the CEMS pattern of a sample prepared with and without applied stress before and after annealing at 473 K. The CEMS patterns were fitted assuming a sextet due to Fe nanocrystals and a doublet due to the amorphous phase. Even in the as-deposited state a sextet with hyperfine field of about 10 Tesla was found to be present. However, the area ratio of this sextate is very small. This indicates that there is a small amount of magnetic alloy while most of the alloy is not ferromagnetic. As the samples were annealed the contribution of this magnetic phase increases indicating an enhancement in the volume fraction of nanocrystalline Fe in agreement with the XRD results. It may be noted that the hyperfine field after annealing remains in the range of

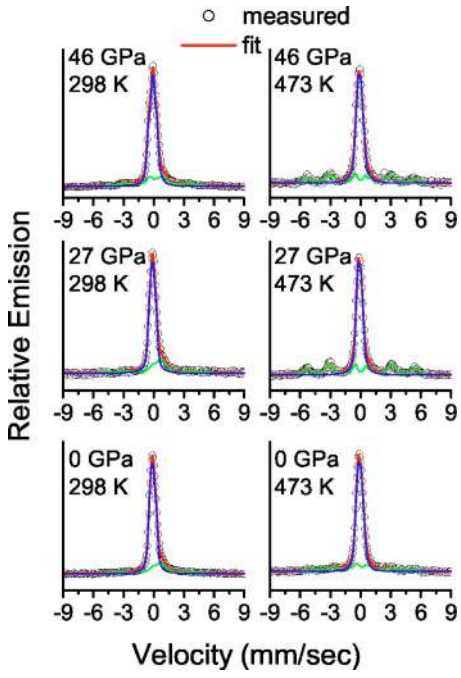

FIG. 7. (Color online) Conversion electron Mössbauer spectroscopy (CEMS) pattern of Si/[$^{natural}Fe_{75}Zr_{25}$(25±1 nm)/$^{57}Fe_{75}Zr_{25}$(12±1 nm)]$_{10}$ multilayer prepared with an applied stress of 0, 27, and 46 GPa in the as-deposited state and after annealing at 473 K.

TABLE I. Fitted CEMS parameters for the sample prepared with and without an applied stress in the as-deposited state and after annealing at 473 K.

Sample	Sample condition	Average hyperfine field (T)	Average quadrupole (mm s^{-1})
0 GPa	As deposited	10.8±0.5 T	0.40±0.01
0 GPa	473 K, 1 h	18.4±1.3 T	0.43±0.01
27 GPa	As deposited	10.2±0.9 T	0.44±0.01
27 GPa	473 K, 1 h	23.4±0.8 T	0.70±0.01
46 GPa	As deposited	13.0±0.2 T	0.44±0.01
46 GPa	473 K, 1 h	22.5±1.5 T	0.42±0.01

18–23 T while that of pure Fe is 33.3 T. The reduced magnetic moment could result due to some thermal fluctuations. Table I compares the fitted values for the different cases as shown in Fig. 7.

MOKE measurements were also performed to understand the changes in the magnetic properties of the system during amorphous to nanocomposite phases. The sample prepared without an applied stress exhibited no anisotropy as a function of an azimuthal angle in the coercivity, while the samples prepared with an applied stress clearly show uniaxial anisotropy, which persists even after the nanocrystallization of the films (see Fig. 8). This confirms that the bending stress induced in the films persists even after nanocrystallization. However, it may be noted that anisotropy is induced even in the stress-free sample after annealing. Therefore it would be difficult to exclude the effect of applied stress.

Formation of a nanocomposite phase after primary crystallization of the amorphous phase is a general phenomenon in amorphous alloys. Often, it was observed that amorphous binary alloys crystallize in two steps. The primary crystallization reaction of most amorphous alloys leads to an evolution of nanocrystalline microstructures whereas the phase formed after the second stage results in an intermetallic compound along with the nanocrystalline phase. The nominal reaction for such a crystallization process had been given as: amorphous $\rightarrow \alpha$+amorphous $\rightarrow \alpha+\beta$; where α is the primary phase that precipitates out from the amorphous matrix and β is an intermetallic compound.[2,11,12] In the present case crystallization of the amorphous phase can be regarded as the primary crystallization process and as evident from the x-ray data, the amorphous phase coexists along with grains of α -Fe. However, the primary crystallization temperature for the present case was found to be very low as compared with $Fe_{67}Zr_{33}$ amorphous alloy.[21] Since in the present case for $Fe_{75}Zr_{25}$ alloy, the Zr content is slightly lower, a decrease in crystallization temperature is not very surprising. In order to further confirm the structure of the alloy, a thin film with even lower Zr content was deposited under identical conditions of sputtering.[27] The composition of this film was $Fe_{80}Zr_{20}$. The XRD pattern of this film showed a narrow peak even in the as-prepared state (not shown in the figure), indicating that the structure forms a nanocrystalline state. Such a decrease in the primary crystallization temperature was also observed in an ion beam sputtered $Fe_{85}Zr_{15}$ sample,[28,29] and a phenomenon analogue to surface crystallization in amorphous alloy ribbons[30–33] was found responsible for early crystallization of amorphous $Fe_{85}Zr_{15}$ film in the thin film state.

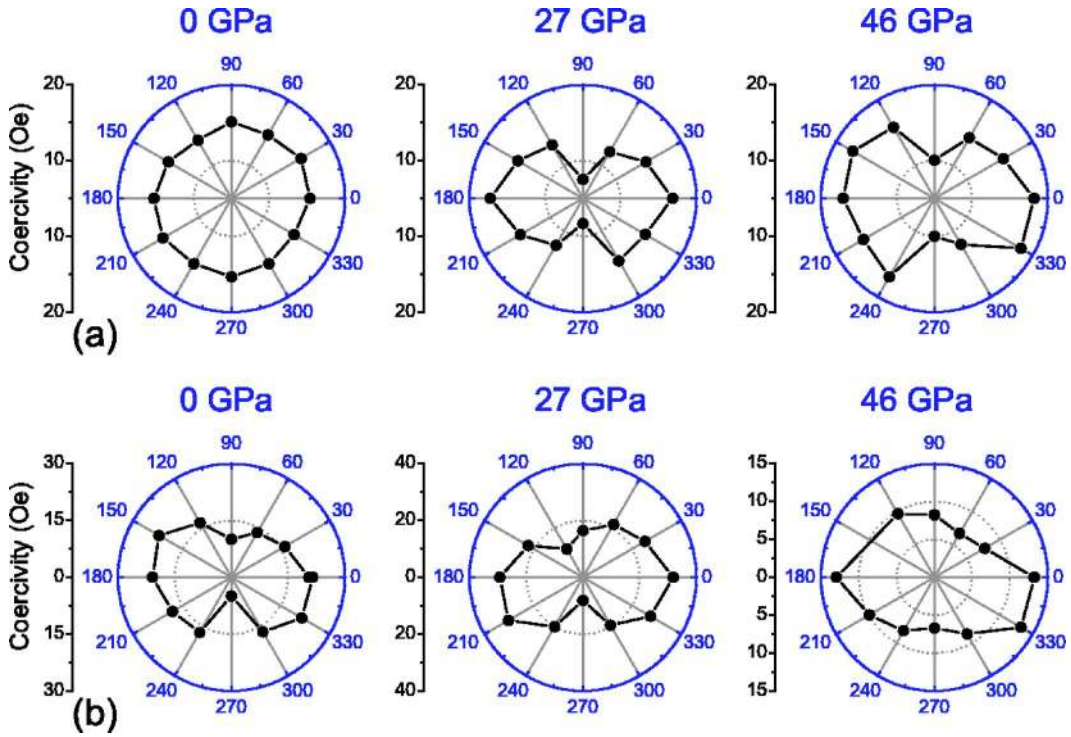

FIG. 8. (Color online) MOKE measurements on Si/[$^{natural}Fe_{75}Zr_{25}$(25±1 nm)/$^{57}Fe_{75}Zr_{25}$(12±1 nm)]$_{10}$ multilayer prepared with an applied stress of 0, 27, and 46 GPa in the as-deposited state (a) and after annealing at 473 K (b).

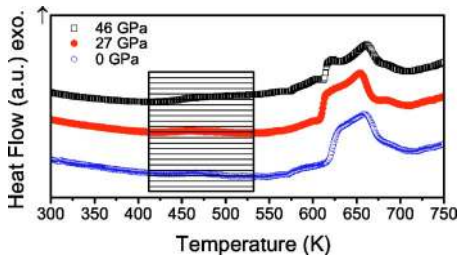

FIG. 9. (Color online) DCS scans of the $Si/[^{natural}Fe_{75}Zr_{25}(25\pm1\ nm)/^{57}Fe_{75}Zr_{25}(12\pm1\ nm)]_{10}$ multilayer prepared with an applied stress of 0, 27, and 46 GPa. The shaded region shown in the figure corresponds to the temperature range used for diffusion measurements.

For the amorphous thin film formed by vapor deposition, the effective quenching rate is very high which results in a higher quenched-in free volume and results in an early crystallization of the amorphous phase as observed in the present case. In order to further understand the crystallization behavior of the alloy, DSC measurements were carried out under a constant heating rate of 0.33 K/s. It was found that a very broad hump appears around 450 K and a relatively sharp peak appears around 613 K in all three samples. The hump appearing at 450 K can be estimated as the first crystallization step while a relatively sharp peak corresponds to a second crystallization step. From the XRD results, the first crystallization event was observed as early as 373 K, where the samples were annealed for 1 h, in the DSC scan since the samples were heated at a much faster rate, the crystallization event was observed at higher temperature as shown in Fig. 9. In a number of studies performed on bulk or thick films (thickness is a few μm), it has been found that the heat release during the first crystallization event is significantly smaller compared to the second crystallization event due to a slower diffusion at lower temperature.[34] In Al-based glasses, Foley *et al.*[35] have studied the crystallization behavior using transmission electron microscopy (TEM) and DSC. While the growth of nanocrystals was confirmed by TEM, there was no evidence of primary crystallization with DSC. Small diffusion of the constituents was argued for the observed behavior. In their case, they observed that, for diffusivity, $D\sim1\times10^{-19}\ m^2\ s^{-1}$, the level of heat output is nearly undetectable in DSC measurements, which requires a signal on the order of 0.1 mW or greater. Unless the value of D is at least two orders of magnitude larger, the signal will be close to the noise level of the DSC (Ref. 35). It may be noted that in the present case, the iron self-diffusivity around 400 K is of the order of $10^{-21}\ m^2\ s^{-1}$ (as shown in later sections). Further, the grain size as determined with XRD results was about 10 nm, the heat release for the formation of small grain sizes is expected to be small. In addition, the DSC measurements in the present case were performed in relatively thin films (370 nm) and the total mass exposed during DSC measurements was only 65 μgm which explains the small heat release during the first crystallization event, in spite of the high sensitivity of the sensor used during DSC measurements. The presence of peaks around 613 K can be understood as a second crystallization step. The onset of a second crystallization temperature was found around (608 ± 5) K for all three samples and there was no systematic effect of applied stress on the second crystallization temperature.

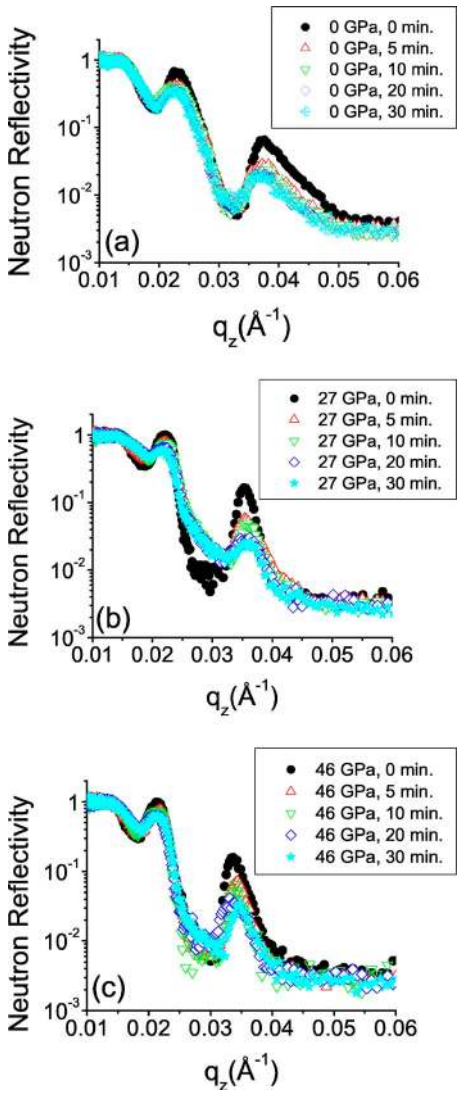

FIG. 10. (Color online) Decay of the Bragg peak intensity as a function of annealing time at 473 K for the sample prepared without an applied stress (a), with an applied stress of 27 GPa (b), and with an applied stress of 46 GPa (c).

C. Self-diffusion measurements, time dependence

With the observed thermal behavior of the samples, for diffusion measurements, a temperature range for diffusion annealing was chosen from 413–533 K in order to study diffusion in the nanocomposite state. This temperature region is also indicated in Fig. 8 as the shaded area. The three samples prepared with an applied compressive stress of 0, 27, and 46 GPa were first pre-annealed at 373 K for 0.5 h to obtain the nanocomposite phase. For studying the time dependence of diffusivity, the samples were further annealed at 473 K and neutron reflectivity measurements were carried out after each annealing. In order to minimize the fluctuations due to a possible variation in the temperature, all the

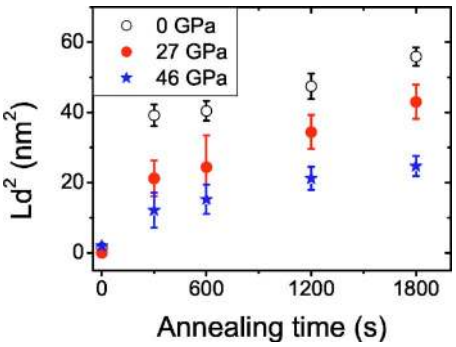

FIG. 11. (Color online) Evolution of diffusion length as a function of annealing time and applied stress at 473 K in nanocomposite Si/[^{natural}Fe$_{75}$Zr$_{25}$(25±1 nm)/^{57}Fe$_{75}$Zr$_{25}$(12±1 nm)]$_{10}$.

samples were annealed simultaneously in the furnace. Figure 10 shows a plot of neutron reflectivities as a function of annealing time at 473 K. A relatively small time step was chosen in order to observe the structural relaxation of the samples. As can be seen from the figure, after annealing, the intensity at the Bragg peak decays. The initial decay was found to be much faster as compared to that with later annealing time. The decay of the Bragg peak intensity can be used to calculate the diffusion coefficient using the expression (Ref. 36):

$$\ln[I(t)/I(0)] = -8\pi^2 n^2 D(T)t/d^2, \tag{3}$$

where $I(0)$ is the intensity before annealing and $I(t)$ is the intensity after annealing time t at temperature T. The diffusion length L_d is related to diffusivity through the relation:

$$L_d = \sqrt{2D(T)t}, \tag{4}$$

where t is the annealing time. The height of the Bragg peak was determined after subtracting the background due to Fresnel reflectivity by multiplying the data by a factor of q^4, where q is the momentum transfer. Figure 11 shows an evolution of the diffusion length as a function of annealing time at 473 K. As can be seen from the figure, the diffusion lengths below an annealing time of 600 s were found to increase much faster as compared to later annealing times. Such behavior in the evolution of the diffusion length was also observed for an $Fe_{67}Zr_{33}$ amorphous sample[21] and is a direct consequence of structural relaxation in the structures.[37,38]

It is interesting to see that for the sample prepared without any stress, the diffusion length increased much faster as compared to the samples prepared with an applied stress. As it is evident from the structural and magnetic measurements, samples prepared with an applied stress exhibited a more relaxed state as compared to that obtained without an applied stress. It is expected that structural relaxation would be more dominant for the sample prepared without an applied stress. The overall magnitude of the diffusion length follows the strength of applied stress and the degree of relaxation is proportional.

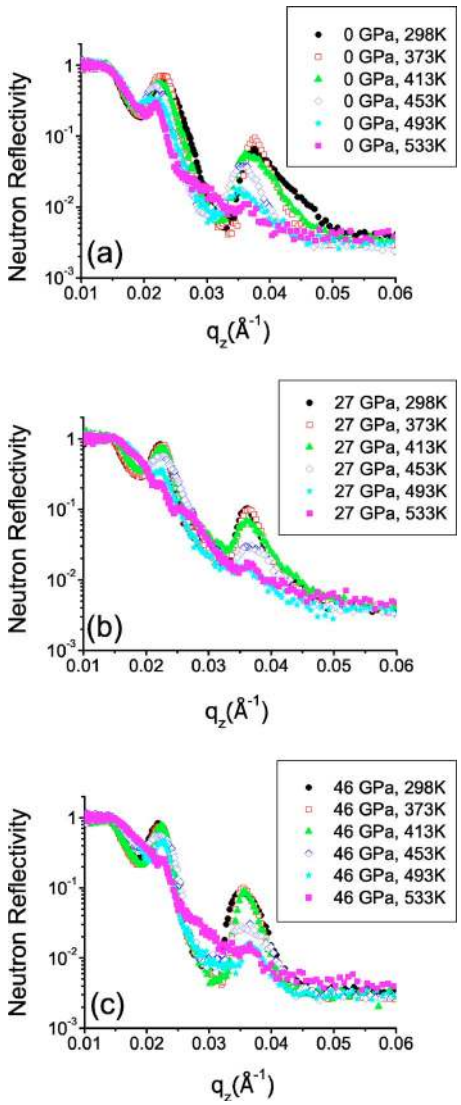

FIG. 12. (Color online) Decay of the Bragg peak intensity as a function of annealing temperature for the sample prepared without an applied stress (a), with an applied stress of 27 GPa (b), and with an applied stress of 46 GPa (c).

D. Self-diffusion measurements, temperature dependence

In order to measure the activation energy for diffusion, the samples were annealed in the temperature range of 413–533 K with a step of 40 K. As can be seen from Fig. 11, after an annealing time of 1800 s, in all cases, the fast relaxation process was almost completed, therefore for the calculation of the activation energy of the system all the samples were annealed for 1800 s at the above mentioned temperatures. It may be noted that annealing for 1800 s may not produce a fully relaxed state of the structure, even though for a comparison of diffusivity for the samples prepared with different applied stress, the time for diffusion annealing was kept constant.

Figure 12 shows the neutron reflectivity pattern obtained after annealing at different temperatures. Again in order to minimize a possible fluctuation in the temperature and annealing conditions, all three samples were annealed simulta-

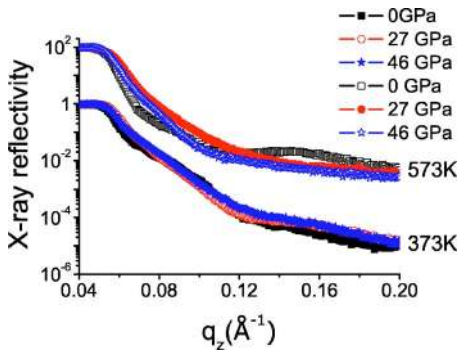

FIG. 13. (Color online) X-ray reflectivity pattern of the Si/[^{natural}$Fe_{75}Zr_{25}$(25±1 nm)/^{57}$Fe_{75}Zr_{25}$(12±1 nm)]$_{10}$ multilayers prepared with and without applied stress after annealing at 373 and 473 K.

neously in the furnace. For a comparison, the neutron reflectivity pattern in the as-prepared state is also shown in the figure. As evident from XRD and CEMS measurements, after annealing the samples undergo from the amorphous to the nanocomposite state, the intensity at the Bragg peaks increases marginally in the neutron reflectivity patterns. In a previous study, it was observed that at the event of primary crystallization in the amorphous $Fe_{67}Zr_{33}$ alloy[21] the neutron reflectivity pattern of an [^{natural}$Fe_{67}Zr_{33}$(9 nm) ^{57}$Fe_{67}Zr_{33}$(5 nm)]$_{20}$ multilayer showed an increase in the intensity at the Bragg peak by a factor as high as 10, as compared to the as-deposited sample. Also the x-ray reflectivity pattern showed an appearance of a Bragg peak due to crystallization accompanied by a phase separation in the alloy.[21] In the present case however, after annealing at 373 K, the amorphous phase nanocrystallizes, but the intensity at the Bragg peak increases only marginally ($<10\%$). Also as shown in Fig. 13, no Bragg peak or structure due to a chemical period appeared up to 573 K in the XRR pattern. This indicates that the primary crystallization behavior of the $Fe_{75}Zr_{25}$ alloy is different as compared to that of the previously studied $Fe_{67}Zr_{33}$ alloy.[21] However, since the matrix obtained after nanocrystallization showed no further significant changes between the temperature range 373–575 K (see also Fig. 8), it is expected that the diffusion process would be not interfered with by structural changes. As shown in Fig. 12, the intensity at both the Bragg peaks decreases with an increase in annealing temperature and after annealing at 533 K, the Bragg peak intensity almost vanishes. This indicates that after annealing at 533 K, both the natural and ^{57}Fe layers are almost completely diffused. With the procedure discussed in the previous section, the diffusivity at each temperature was obtained. Figure 14 shows a plot of diffusivity obtained with both the Bragg peaks for the three samples. As can be seen from the figure, both the Bragg peaks yield similar diffusivity within the experimental errors. The error bars in the present case are basically representing the errors in determining the height of the Bragg peaks obtained from a peak fitting procedure.

The values for the diffusivity obtained for the three samples at the above mentioned temperatures (along with the separately annealed samples at 473 K) could be fitted to the

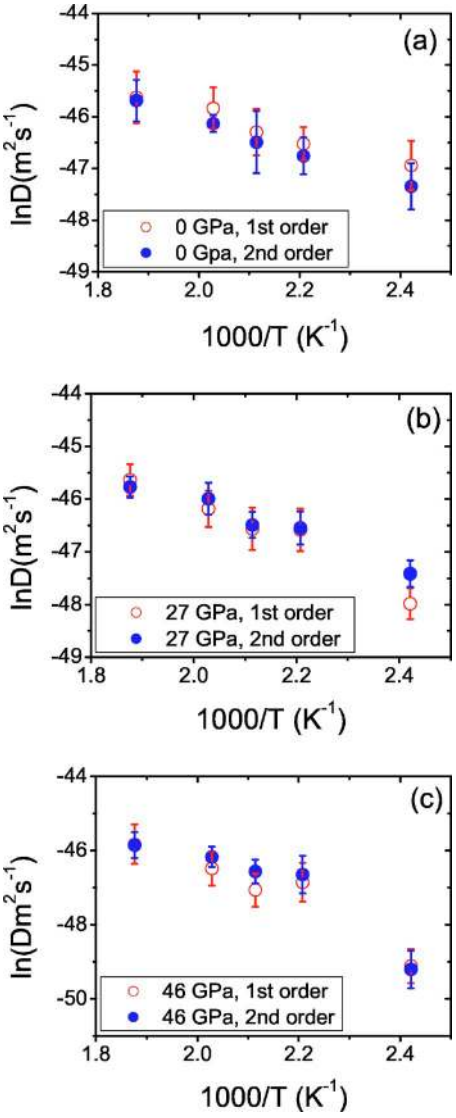

FIG. 14. (Color online) Arrhenius behavior of the diffusivity obtained from the first and second order Bragg peaks for samples prepared with an applied stress of 0 GPa (a), 27 GPa (b), and 46 GPa (c).

relation $\ln D = \ln D_0 - (E/k_BT)$, where D_0, E, and T are the pre-exponential factor, the activation energy, and the annealing temperature, respectively and k_B is the Boltzmann constant. In all three cases the logarithm of diffusivity follows Arrhenius behavior and accordingly, the activation energy and the pre-exponential factor for iron self-diffusion in the $Fe_{75}Zr_{25}$ alloy was obtained. The observed values of both the E and D_0 are given in Table II along with the values obtained for the amorphous $Fe_{67}Zr_{33}$ alloy. Figure 15 shows a plot of diffusivity obtained from the first order Bragg peak for the sample at 0, 27, and 46 GPa. The activation energy was found to increase with an increase in the strength of applied compressive stress (a steeper slope was observed with an increase in the applied stress). The result gives a clear indication that diffusivity for the sample prepared with applied stress is much slower as compared with that prepared without an applied stress. This result also supports the time de-

TABLE II. Activation energy and the pre-exponential factor for iron self-diffusion in nanocrystalline Si/[^{natural}Fe$_{75}$Zr$_{25}$(25±1 nm)/^{57}Fe$_{75}$Zr$_{25}$(12±1 nm)]$_{10}$ multilayers as a function of applied stress during sample preparation. Both the activation energy and the prefactor represent the statistical averaged values obtained from the first and second order Bragg peaks.

Sample	Sample condition	Activation energy (E, eV)	Prefactor (D_0, m^2 s^{-1})
Nano.-Fe$_{75}$Zr$_{25}$	0 GPa	0.24±0.05	$3\times10^{-18\pm1}$
Nano.-Fe$_{75}$Zr$_{25}$	27 GPa	0.31±0.05	$1\times10^{-17\pm1}$
Nano.-Fe$_{75}$Zr$_{25}$	46 GPa	0.51±0.05	$1\times10^{-15\pm1}$
Amorphous-Fe$_{67}$Zr$_{33}$	0 GPa	0.38±0.05	$3\times10^{-18\pm1}$

pendence of the diffusivity as shown in Fig. 11.

In an earlier study Klugkist *et al.*[39–41] studied Co and Zr self-diffusion in amorphous CoZr alloy using a radioactive tracer method as a function of pressure and temperature dependence. It was found that the pressure dependence for Co self-diffusion is extremely small while for Zr self-diffusion it is of the order of one activation volume. On the basis of obtained results it was concluded that Zr diffuses via thermal defects, whereas vacancylike thermal defects can be ruled out for Co self-diffusion. However, our results clearly indicate a decrease in diffusivity with an increase in applied stress. Here we would like to point out that a direct comparison between the studies performed earlier[39,40] with that of our results could not be made. The following points are important to understand our results. (i) The neutron reflectometry technique offers a depth resolution in a subnanometer range; it is possible to measure the initial stage of self-diffusion in a alloy unlike conventional techniques, e.g., SIMS or a radioactive tracer method, however, the information obtained is averaged over the whole sample. (ii) As mentioned already in our case, the alloy could have not attained a fully relaxed state as pre-annealing time was very short compared with that in the literature. (iii) The applied stress is uniaxial and there could be a stress gradient parallel to the surface normal, however, care was taken to select an area of the sample where the gradient is expected to be minimum. Combining the above mentioned points, it is not surprising that there is a strong dependence of self-diffusion of Fe on applied stress, which points out that in the initial state the diffusion mechanism could be different.

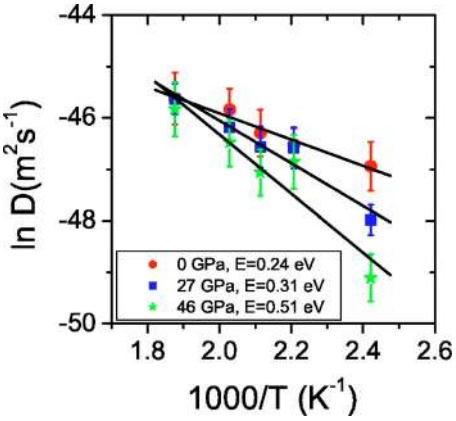

FIG. 15. (Color online) Activation energy and pre-exponential factor for diffusion as a function of applied stress in Si/[^{natural}Fe$_{75}$Zr$_{25}$(25±1 nm)/^{57}Fe$_{75}$Zr$_{25}$(12±1 nm)]$_{10}$ multilayer. The data correspond to the diffusivity obtained from the first order Bragg peak. The sample prepared with the highest applied stress gives an activation energy more than twice as compared with the sample prepared without an applied stress. The detailed values of activation energy and the pre-exponential factors are given in Table II.

Comparing the diffusivity for the sample prepared at 0 GPa with that of the amorphous Fe$_{67}$Zr$_{33}$ sample (also prepared at 0 GPa), the diffusivity in the nanocomposite state is slightly higher as compared to the amorphous sample. The activation energy for the nanocomposite sample was lower by 0.14 eV, while the pre-exponential factors were found to be exactly similar (see Table II). An enhancement in diffusivity in the nanocomposite state is not unexpected due to presence of grains and grain boundaries (GB), while the amorphous phase is expected to be free from grains and GBs. However, the enhancement in diffusivity in the present case is not as spectacular as observed, e.g., in the FINEMET type nanocrystalline-Fe$_{73.5}$Si$_{13.5}$B$_9$Nb$_3$Cu$_1$ in which the Fe self-diffusion showed a large enhancement over that in the parent amorphous phase.[42,43] It may be noted that in the present case the composition of the nanocomposite Fe$_{75}$Zr$_{25}$ alloy is also not similar to the amorphous Fe$_{67}$Zr$_{33}$ alloy, therefore an enhancement in diffusivity may also occur due to increased concentration of Fe. In another study self-diffusion of iron was measured in the parent amorphous and nanocomposite Fe$_{85}$Zr$_{15}$ alloy thin film produced by ion-beam sputtering. It was found that iron self-diffusion in both the amorphous and nanocomposite states was similar and found to occur exclusively through the GB regions which were amorphous in nature.[28] In the present case as well the GBs in the nanocomposite state are amorphous, which might happen due to the fact that in the nanocomposite state, the structure consists of a mixture of nanocrystalline grains of Fe and the remaining amorphous phase. The nanocrystalline grains of Fe would be surrounded by amorphous GBs and in such a situation a percolating path between the nanocrystals may not establish and diffusivity in the nanocomposite phase would be similar to that in the amorphous state.

On the other hand, the activation energy obtained for the sample prepared with the highest applied stress was found to be larger (slower diffusivity) as compared to the amorphous Fe$_{67}$Zr$_{33}$ sample. This is somewhat surprising as the sample prepared even at the highest stress is also in the nanocomposite state. In case the diffusion mechanism is dominated by grains and GBs the effective applied stress should result in an enhancement of the diffusivity.[44] As discussed earlier, an applied compressive stress produced a more relaxed state of the sample as compared to samples prepared without stress. If the diffusion mechanism is dominated by a somewhat collective type migration of atoms both in the amorphous and nanocomposite cases, annihilation of free volume would result in a diffusion mechanism involving a small group of atoms.

IV. CONCLUSIONS

In the present work, the effect of compressive stress on self-diffusion of iron in chemically homogeneous multilayers of FeZr/^{57}FeZr was investigated. It was found that samples in the as-prepared state were amorphous and undergo primary crystallization when annealed at 373 K. The diffusion measurements were performed in the nanocomposite state and it was observed that with an increase in the strength of applied stress, there is a significant increase in the activation energy.

ACKNOWLEDGMENTS

The authors would like acknowledge: A. Foelske, General Energy Research, Paul Scherrer Institute, for providing help in x-ray photoelectron spectroscopy measurements; and K. Conder, P. Keller, and M. Horisberger, Laboratory for Neutron Scattering, Paul Scherrer Institute for providing help in DSC measurements, manufacturing of the three-point Si wafer bending machine; and assisting in thin film deposition, respectively. A part of this work was performed at the Swiss Spallation Neutron Source, Paul Scherrer Institute, Villigen, Switzerland.

*Corresponding author. Present address: UGC-DAE Consortium for Scientific Research, Mumbai Centre, BARC, Mumbai 400085, India. Email address: mgupta@csr.ernet.in

[1] P. G. Debenedetti and F. H. Stillinger, Nature (London) **410**, 259 (2001).
[2] C. A. Angell, K. L. Ngai, G. B. McKenna, P. F. McMillan, and S. Martin, J. Appl. Phys. **88**, 3113 (2000).
[3] M. E. McHenry, M. A. Willard, and D. E. Laughlin, Prog. Mater. Sci. **44**, 291 (1999).
[4] A. Dunlop, G. Jaskierowicz, G. Rizza, and M. Kopcewicz, Phys. Rev. Lett. **90**, 015503 (2003).
[5] E. Ma, Nat. Mater. **2**, 7 (2002).
[6] A. Kojima, A. Makino, and A. Inoue, J. Appl. Phys. **87**, 6576 (2000).
[7] A. Kojima, F. Ogiwara, A. Makino, A. Inoue, and T. Masumoto, Mater. Sci. Eng., A **226-228**, 520 (1997).
[8] X. Y. Zhang, Y. Guan, J. W. Zhang, W. Sprengel, K. J. Reichle, K. Blaurock, K. Reimann, and H.-E. Schaefer, Phys. Rev. B **66**, 212103 (2002).
[9] B. B. Kappes, B. E. Meacham, Y. L. Tang, and D. J. Branagan, Nanotechnology **14**, 1228 (2003).
[10] W. J. Botta, F. D. Negri, and A. R. Yavari, J. Non-Cryst. Solids **247**, 19 (1999).
[11] K. Hono and D. H. Ping, Mater. Charact. **44**, 203 (2000).
[12] D. M. Zhu, K. Raviprasad, K. Suzuki, and S. P. Ringer, J. Phys. D **37**, 645 (2004).
[13] Y. Yoshizawa, S. Oguma, and K. Yamauchi, J. Appl. Phys. **64**, 6044 (1988).
[14] K. Suzuki, A. Makino, N. Kataika, A. Inoue, and T. Masumoto, Mater. Trans., JIM **32**, 93 (1991).
[15] M. A. Willard, M.-Q. Huang, D. E. Laughlin, M. E. McHenry, J. O. Cross, V. G. Harris, and C. Franchetti, J. Appl. Phys. **85**, 4421 (1999).
[16] F. Faupel, W. Frank, M. P. Macht, H. Mehrer, K. Rätzke, H. R. Schober, S. K. Sharma, and H. Teichler, Rev. Mod. Phys. **75**, 237 (2003).
[17] R. Abermann and R. Koch, Thin Solid Films **129**, 71 (1985).
[18] A. L. Shull and F. Spaepen, J. Appl. Phys. **80**, 6243 (1996).
[19] J. Floro, S. J. Hearne, J. A. Hunter, P. Kotula, E. Chason, S. C. Seel, and C. V. Thompson, J. Appl. Phys. **89**, 4886 (2001).
[20] R. Koch, J. Phys.: Condens. Matter **6**, 9519 (1994).
[21] M. Gupta, A. Gupta, J. Stahn, M. Horisberger, T. Gutberlet, and P. Allenspach, Phys. Rev. B **70**, 184206 (2004).
[22] G. G. Stoney, Proc. R. Soc. London, Ser. A **82**, 172 (1909).
[23] J. Chen and I. D. Wolf, Semicond. Sci. Technol. **18**, 261 (2003).
[24] M. Gupta, T. Gutberlet, J. Stahn, P. Keller, and D. Clemens, Pramana, J. Phys. **63**, 57 (2004).
[25] L. Parratt, Phys. Rev. **95**, 359 (1954).
[26] A. Guinier, *X-Ray Diffraction: In Crystals, Imperfect Crystals and Amorphous Bodies* (Dover, New York, 1994).
[27] M. Gupta, R. Gupta, A. Gupta, and T. Gutberlet (unpublished).
[28] A. Gupta, M. Gupta, U. Pietsch, S. Ayachit, S. Rajagopalanl, A. K. Balamurgan, and A. K. Tyagi, J. Non-Cryst. Solids **343**, 39 (2004).
[29] M. Gupta and A. Gupta, Phys. Status Solidi C **1**, 3211 (2004).
[30] A. Gupta, S. Habibi, S. Lal, and G. Principi, Hyperfine Interact. **55**, 967 (1990).
[31] A. P. Radlinski, A. Calka, and B. Luther-Davies, Phys. Rev. Lett. **57**, 3081 (1986).
[32] P. R. Rao, Rev. Solid State Sci. **3**, 311 (1989).
[33] U. Köster and B. Punge-Witteler, Mater. Res. Soc. Symp. Proc. **80**, 355 (1987).
[34] J. H. Perepezko, R. J. Hebert, R. I. Wu, and G. Wilde, J. Non-Cryst. Solids **317**, 52 (2003).
[35] J. C. Foley, D. R. Allen, and J. H. Perepezko, Scr. Mater. **35**, 655 (1996).
[36] J. Speakman, P. Rose, J. A. Hunt, N. Cowlam, R. E. Somekh, and A. L. Greer, J. Magn. Magn. Mater. **156**, 411 (1996).
[37] Y. Loirat, J. L. Boequet, and Y. Limoge, J. Non-Cryst. Solids **265**, 252 (2000).
[38] M. Gupta, A. Gupta, S. Rajagopalan, and A. K. Tyagi, Phys. Rev. B **65**, 214204 (2002).
[39] P. Klugkist, K. Rätzke, S. Rehders, P. Troche, and F. Faupel, Phys. Rev. Lett. **80**, 3288 (1998).
[40] P. Klugkist, K. Rätzke, and F. Faupel, Phys. Rev. Lett. **81**, 614 (1998).
[41] P. Klugkist, K. Rätzke, F. Faupel, P. Torche, F. Fielitz, and V. Naundorf, Philos. Mag. Lett. **79**, 827 (1999).
[42] H. Tanimoto, P. Farber, R. Würschum, R. Z. Valiev, and H. E. Schaefer, Nanostruct. Mater. **12**, 681 (1999).
[43] R. Würschum, P. Farber, R. Dittmar, P. Scharwaechter, W. Frank, and H.-E. Schaefer, Phys. Rev. Lett. **79**, 4918 (1997).
[44] K. M. Crosby, cond-mat/0307065 (unpublished).